Estimation of Eddy Dissipation Rates from Mesoscale Model Simulations

Nash'at N. Ahmad[*], Fred H. Proctor[†]
NASA Langley Research Center, Hampton, Virginia, 23681

The Eddy Dissipation Rate is an important metric for representing the intensity of atmospheric turbulence and is used as an input parameter for predicting the decay of aircraft wake vortices. In this study, the forecasts of eddy dissipation rates obtained from the current state-of-the-art mesoscale model are evaluated for terminal area applications. The Weather Research and Forecast mesoscale model is used to simulate the planetary boundary layer at high horizontal and vertical mesh resolutions. The Bougeault-Lacarreré and the Mellor-Yamada-Janjić schemes implemented in the Weather Research and Forecast model are evaluated against data collected during the National Aeronautics and Space Administration's Memphis Wake Vortex Field Experiment. Comparisons with other observations are included as well.

I.   Introduction

DECAY and transport of aircraft wake vortices depend on the strength of the ambient atmospheric turbulence, among other factors. Current fast-time wake transport and decay prediction models (Sarpkaya et al. 2001; Holzapfel and Robins 2004; Proctor et al. 2006; Proctor 2009) use eddy dissipation rate (EDR) as the parameter that controls the decay of wake vortices due to atmospheric turbulence. The EDR can be obtained from wind data measured at high frequency with various sensors such as sonic anemometers. However, the cost of deploying a comprehensive array of sensors that can adequately cover the entire spatial extant of an airport terminal area is prohibitive and therefore measurements can be taken at the most at few points in space. Another disadvantage is the problem of providing forecasts of EDR for several hours following the measurement time. Weather forecasts for supporting the terminal area operations can be obtained with the help of numerical models and substantial progress has been made in mesoscale modeling over the last three decades. The operational models include the National Center for Atmospheric Research's (NCAR) Weather Research and Forecasting (WRF) model (Klemp et al. 2007), Science Applications International Corporation's Operational Multiscale Environment model with Grid Adaptivity (Bacon et al. 2000), the United States Navy's Coupled Ocean/Atmosphere Mesoscale Prediction System (Hodur 1997), the Mesoscale Atmospheric Simulation System (MASS) model (Meso, Inc. 1995), the Mesoscale Model 5 (MM5) developed jointly by the Pennsylvania State University and the National Center for Atmospheric Research (Dudhia 1993) and the National Centers for Environmental Prediction's (NCEP) Rapid Update Cycle (RUC) developed by Benjamin et al. (2004).

There are many challenges in using mesoscale models for wake vortex applications. First, the computational cost of running the models at an appropriate spatial and temporal resolution for wake applications can be prohibitive. A fine mesh-resolution can be achieved in the vertical, but a practical resolution in the horizontal is limited to between 4*km* and 10*km*. The restriction on horizontal mesh resolution is due to computational constraints as well as the validity of various physics parameterizations used in the model. This horizontal resolution can, at best, resolve the whole terminal area by just a few grid points (Figure 1). The use of coarse grid resolution for wake applications can introduce uncertainties in the forecast of winds and turbulence quantities. Secondly, the physics parameterizations in mesoscale models are scale specific which makes it difficult to simulate complex atmospheric phenomenon that are inherently multiscale. The grid resolution related uncertainties are in addition to the uncertainties due to the nonlinearity of the governing equation set solved by the models. Another uncertainty in model forecasts is due to inadequate initial and boundary conditions.

---

[*] Research Aerospace Engineer, NASA, Hampton, Virginia. Senior Member, AIAA.
[†] Senior Research Scientist, NASA, Hampton, Virginia. Senior Member, AIAA.

Some recent applications of mesoscale modeling to support terminal area operations in general and wake vortex research in particular include: Kaplan et al. (1999), Charney et al. (2000), Kaplan et al. (2006), Frech et al. (2007), and Ringley et al. (2007). These studies have had mixed results in terms of success in predicting winds, temperature and turbulence quantities. Temperature predictions usually had the least amount of error, whereas, the EDR obtained from the turbulence kinetic energy (TKE) predictions were either significantly overestimated or underestimated.

In this study, the National Center for Atmospheric Research (NCAR) state-of-the-art mesoscale model is evaluated as a tool for providing forecasts of EDR. The model forecasts are compared against data observed at Memphis International Airport during the month of August in 1995. This data was collected during the Memphis Wake Field Experiment which was sponsored by the National Aeronautics and Space Administration (NASA) during the month of August in 1995. In the following sections the Memphis Field Experiment is described briefly and the results of the WRF simulations are discussed in detail.
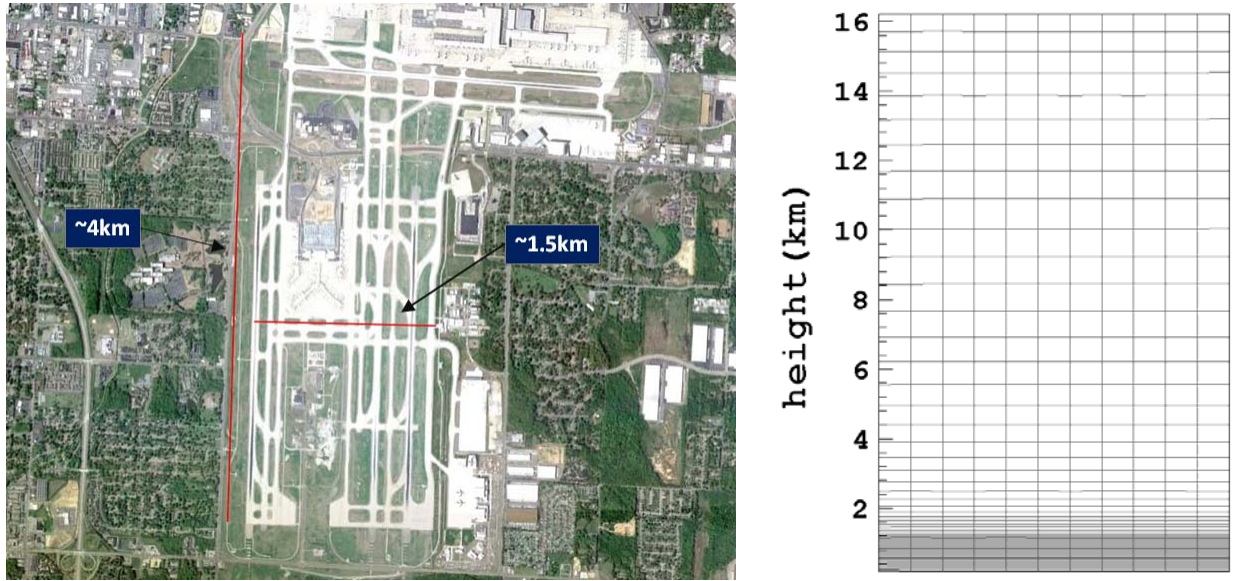

Figure 1. Memphis International Airport is shown in the left panel and its approximate length and width is marked on the figure. The horizontal mesh resolution of mesoscale models is usually on the order of a few kilometers and at best can represent the entire airport by a few points. In the vertical, however a high-resolution can be prescribed. The grid shown in the right panel has a resolution of 40m in the boundary layer. Above the boundary layer the grid is stretched all the way to the top of the computational domain.

II.   Eddy Dissipation Rate

According to Kolomogrov's hypothesis, the large eddies in the atmosphere are inherently unstable. These large eddies break up and transfer their energy to smaller-sized eddies. This transfer or "cascade" of energy continues from larger to smaller eddies, until viscous dissipation becomes dominant and the TKE is converted into heat. The rate at which the TKE is dissipated is known as the EDR. In other words, EDR is the rate at which the TKE is absorbed by breaking down eddies into smaller and smaller eddies until it is converted into heat by viscous forces (Figure 2). The length scale of the large energy containing eddies, l_0, also known as the integral scale of the turbulence, can be derived as follows:

$$l_0 \propto \frac{e^{3/2}}{\varepsilon} \tag{1}$$

where, ε is the eddy dissipation rate in m^2/s^3. The turbulence kinetic energy, e in m^2/s^2 is given by:

$$e = \frac{1}{2}\left(\overline{u'^2} + \overline{v'^2} + \overline{w'^2}\right) \tag{2}$$

In Eq. (2), u', v', w' are the turbulent fluctuations of u, v, and w-velocity components from some time-averaged mean value and the bar symbol denotes time averages.

Re-arranging Eq. (1) gives:

$$\varepsilon = \frac{Ce^{3/2}}{l_0} \tag{3}$$

where, C is a proportionality constant of order one. The eddy dissipation rates can be estimated directly from high frequency wind measurements (e.g., Campbell et al. 1997) and from similarity theory (Han et al. 2000).

In mesoscale models, EDR can be diagnosed from the model's TKE closure schemes that are used for computing subgrid scale processes. The accuracy of the TKE predictions and EDR calculations depend on the underlying assumptions and approximations in the particular TKE closure scheme used by the model. Since the TKE is a standard output of most mesoscale models, the unknowns left in Eq. (3) are the integral length scale, l_0, and the proportionality constant, C. Eq. (3) is sometimes further simplified as follows:

$$\varepsilon = \frac{e^{3/2}}{L_e} \tag{4}$$

where the proportionality constant, C, and the integral length scale, l_0, have been combined into a length scale, L_e, that needs to be specified.

Gerz et al. (2005) have developed the Nowcasting Wake Vortex Impact Variables (NOWVIV) model to forecast the cross winds and turbulence quantities for supporting wake vortex studies. The NOWVIV tool is built upon the MM5 model with a level-3 turbulence closure scheme (Burk and Thompson 1989). In one of their studies, Frech et al. (2007) have evaluated the EDR predictions obtained from the NOWVIV model. The inner-most nest in their study had a horizontal grid resolution of $2.1km$ and a stretched vertical grid that placed 26 of the 60 vertical levels below $1100m$. Frech et al. (2007) defined L_e equal to a constant $311m$ and found that resulting EDR values were underestimated above an altitude of $100m$. They suggested using direct model outputs of EDR for heights above $100m$ and TKE-derived estimates below $100m$. Ringley et al. (2007) assumed $L_e = 336m$ (instead of $311m$), which was based on their analysis of $40m$ wind observations. In their study, the EDR was overestimated by one or two orders of magnitude near the surface, whereas the predictions at an altitude of $40m$ compared well with observations. Kaplan et al. (2006) used the MASS model to run simulations on a fine-scale mesh resolution that assumed a horizontal grid spacing of $167m$ and 60 vertical levels below $2km$. In Kaplan et al. (2006), the length scale, L_e, was calculated as a function of Richardson number (Therry and Lacarreré 1983; and Bougeault and Lacarreré 1989) and the EDR estimates compared well with the observations. Charney et al. (2000) used similarity theory (Han et al. 2000) to estimate EDR and TKE. This methodology, however, significantly overestimated the EDR.
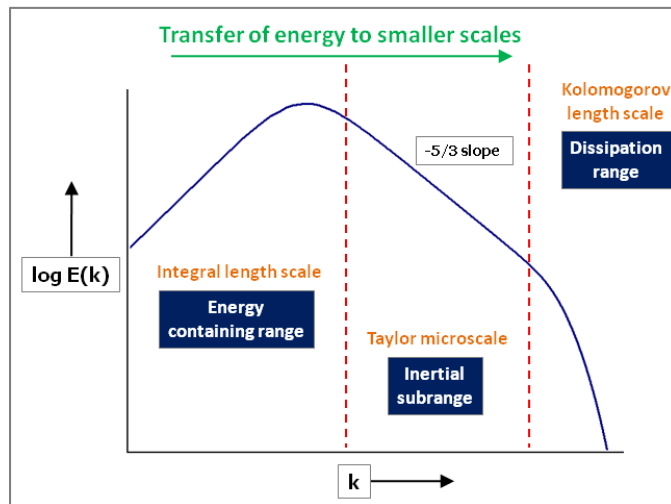

Figure 2. The Kolomogrov Energy Spectrum. Energy range for eddies of different sizes and their associated length scales are shown in the figure as a function of wavelength.

American Institute of Aeronautics and Astronautics

III.   The Memphis Wake Vortex Field Experiment

A comprehensive field experiment to measure wake vortices and the ambient meteorological conditions was conducted at the Memphis International Airport in Memphis, Tennessee from August 6 through August 29, 1995 (Campbell, et al. 1997). The experiment was sponsored under NASA Langley Research Center's Aircraft Vortex Spacing System (AVOSS) project (Hinton 1995; Perry et al. 1997). Several sensor systems were deployed to collect detailed meteorological data to study the effect of atmospheric conditions on the behavior of wake vortices. The sensors included radiosondes, sodars, a wind profiler, one $150ft$ high meteorological tower, a radio acoustic sounding system (RASS) and NASA Langley's OV-10 research aircraft. The radiosondes were used to measure winds and temperature measurements ($10s$ averages) at $50m$ vertical resolution. The OV-10 aircraft was flown at selected times and took measurements of temperature and winds at a sample rate of $10Hz$. Temperature ($5min$ averages) was measured using RASS every $30min$ at 97 vertical levels from $145m$ to $1492m$. The $150ft$ ($45.7m$) meteorological tower (located at latitude 35.029167°N and longitude 89.981111°W and an elevation of $97.37m$ above sea level) was equipped with a large array of sensor systems (Table 1). Winds, temperature and moisture were measured from the tower at $5m$, $10m$, $20m$, $30m$, and $42m$ heights. Turbulence quantities (TKE and EDR) were estimated from wind measurements at $5m$ and $40m$ heights. Rain rate, soil temperature, soil moisture, barometric pressure and incoming and outgoing solar radiation also were measured by the sensors deployed on the meteorological tower. In addition to the tower data, standard meteorological data such as atmospheric pressure, temperature, moisture, cloud cover, and visibility, etc. was obtained from the National Weather Service's Surface Aerodrome Observations (SAO) and the Automated Surface Observations System (ASOS). Figure 3 shows some of the sensors deployed at the Memphis International Airport during the field experiment.

Figure 3. Memphis Wake Vortex Field Experiment. A B757 landing in the background of the NASA lidar van (top left); profiler (top right); Michael Mathews (left) and Dr. Fred Proctor (right) standing next to the radiometer mounted at the base of the meteorological tower (bottom left); and Dr. Tim Dasey in the lidar van (bottom right).

Table 1: Data Collection by the 150*ft* Meteorological Tower

Measured Quantity	Height (m)	*f* (Hz)	Averaging Time	Sensor System	Accuracy
temperature (°C)	5, 10, 20, 30, 42	1	1 min	SAVPAK	0.3°C
relative humidity (%)	5, 10, 20, 30, 42	1	1 min	SAVPAK	3%
wind speed (m/s)	5, 10, 20, 30, 42	1	1 min	SAVPAK	2%
wind direction (degrees)	5, 10, 20, 30, 42	1	1 min	SAVPAK	1 degree
virtual temperature (K)	5, 40	10	1 min	FLUXPAK	0.05°C
u-velocity (m/s)	5, 40	10	1 min	FLUXPAK	0.05m/s
v-velocity (m/s)	5, 40	10	1 min	FLUXPAK	0.05m/s
w-velocity (m/s)	5, 40	10	1 min	FLUXPAK	0.05m/s
pressure (mb)	2	1	1 min	BAROMETER	0.15mb
net radiation (W/m^2)	2	1	1 min	RADIOMETER	n/a
incoming radiation (W/m^2)	2	1	1 min	RADIOMETER	n/a
outgoing radiation (W/m^2)	2	1	1 min	RADIOMETER	n/a
soil temperature (°C)	10cm below ground	1	1 min	SOILPAK	0.05°C
soil moisture (%)	10cm below ground	1	1 min	SOILPAK	n/a
accumulated rain (inches)	2	n/a	1 min	SOILPAK	0.01in

In order to compare the model predictions with the observed data, a period was selected for the numerical simulations from August 15 through August 20, 1995, which coincided with the times that observed data was collected during AVOSS. During the August 1995 field experiment, the weather conditions followed the typical summertime pattern for the Memphis area. The days were hazy, hot, and humid with generally light winds (Campbell et al. 1997; Zak 1995). The atmosphere in the nighttime was hazy, warm and very humid with light winds (Campbell et al. 1997; Zak 1995). The observed daily maximum and minimum temperatures, dew point temperatures, and maximum wind speed at 5*m* were obtained from SAVPAK and are listed in Table 2. The sunrise and sunset times for the period of interest are also listed in Table 2. The values in Table 2 reflect this pattern with the exception of August 19. The large wind speed recorded on August 19 is due to a gust front that moved through the airport. Precipitation was recorded on August 17 and August 19, from thunderstorms that developed nearby during the late afternoon and the evening hours.

Table 2: Some Observations at Memphis, Tennessee

date	sunrise	sunset	min T(°F)	max T(°F)	min T$_d$(°F)	max T$_d$(°F)	max wspd (*m/s*)
19950815	0619CDT	1949CDT	76.19	92.12	69.78	76.78	4.75
19950816	0620CDT	1948CDT	76.46	94.37	71.71	77.12	4.67
19950817	0621CDT	1947CDT	77.99	96.06	72.95	80.15	6.89
19950818	0621CDT	1945CDT	77.63	97.14	71.04	77.59	6.33
19950819	0622CDT	1944CDT	73.36	95.79	66.68	80.45	18.38
19950820	0623CDT	1943CDT	SAVPAK data was not available for this date				

Central Daylight Time (CDT) = Coordinated Universal Time (UTC) – 5*hr*

IV.   Mesoscale Modeling

The WRF model (Klemp et al. 2007) is a mesoscale weather prediction model that has been developed by NCAR with help from various partners in academia and federal research laboratories. It has governing equations for the time-dependent, three-dimensional, nonhydrostatic, fully compressible Navier-Stokes equations. The model grid structure is based on Arakawa C-grid staggering (Arakawa and Lamb 1977). In the vertical, WRF uses a terrain-following pressure formulation, where the top of the domain is a constant pressure surface. The mesh can be stretched in the vertical to provide higher resolution in the boundary layer. One-way and two-way nesting options are available to provide high horizontal grid resolution in regions of interest. The horizontal and vertical advection terms can be discretized anywhere from second to sixth-order spatial accuracy. Fifth-order upwind differencing in the horizontal direction and third-order upwind differencing in the vertical direction are recommended by the developers of the WRF model. The time integration is done using an explicit third-order Runge-Kutta time marching scheme, with smaller time steps for acoustic and gravity wave modes. Monotonic as well as positive-definite schemes can be used for the advection of microphysical scalars, chemical scalars and TKE. High resolution terrain and other land use datasets are part of the standard WRF distribution.

Extensive physics packages for modeling the surface layer interactions, boundary layer turbulence processes and cumulus parameterizations have been implemented in the model. Twelve different cloud microphysics schemes of varying complexity are available, as well as parameterizations for radiation physics (four different schemes for longwave radiation and seven schemes for shortwave radiation). The user has the choice of six schemes for surface layer interactions. Nine different schemes have been implemented in the WRF model for the parameterization of sub-grid scale diffusion processes in the planetary boundary layer (PBL). The schemes vary in complexity and range from simple non-local-K schemes (e.g., Troen and Mahrt 1986) to large eddy simulation (LES) for very high resolution grids. The LES option in WRF has not been extensively tested or used. There are a number of TKE-based closures implemented in the WRF model (Janjić 1994; Bougeault and Lacarreré 1989; Nakanishi and Niino 2004). The TKE-closure schemes implemented in many mesoscale models are usually some variant of the Mellor-Yamada scheme (Mellor and Yamada 1982), in which the prognostic equation for the TKE is computed.

In this study, the Mellor-Yamada-Janjić scheme (Janjić 1994) was used, which is a variant of the Level 2.5 Mellor-Yamada turbulence scheme. The Mellor-Yamada scheme in its original form is singular in the limit of vanishing shear. The Mellor-Yamada-Janjić (MYJ) scheme is an improved version of the Mellor-Yamada scheme that remedies the singularity problem. In addition to the MYJ PBL scheme, the Bougeault and Lacarreré (BL) scheme was also evaluated. The BL scheme is 1.5 order and solves the prognostic equation for the TKE. The specification of the length scale and other constants in the BL PBL scheme is discussed in Bougeault and Lacarreré (1989). The MYJ PBL scheme is described in detail in Janjić (2001). When these two PBL schemes are used, the WRF model output consists of TKE and the master length scale which are then used to compute the EDR in the post-processing step.

V.   Simulations Results

In this section the results of WRF simulations are discussed in detail. Six days of simulations were performed from August 15 to August 20, 1995 using the two different PBL schemes. Prior to these simulations, a detailed sensitivity study was conducted to evaluate the effect of various WRF input parameters. The results were compared with available surface and upper air observations.

A. Simulations Setup and Summary

Three levels of grid nesting were utilized in the simulations in order to achieve acceptable grid resolution while maintaining computational efficiency. The WRF simulation domain consisted of an outer most domain bounded between 124.06°W and 55.93°W in the longitude and 18.08°N and 49.14°N in the latitude with a horizontal mesh resolution of 36km. Two higher resolution nests were defined within the outermost domain. Domain 2 was bounded between 111.54°W and 68.45°W in the longitude and 24.84°N and 43.86°N in the latitude with a horizontal mesh resolution of 12km. The innermost domain was bounded between 99.74°W and 79.97°W in the longitude and 30.66°N and 39.29°N in the latitude with a horizontal mesh resolution of 4km. High-resolution (1km) terrain and land use datasets were used for the innermost domain while lower resolution terrain was used in the coarser nests. The WRF computational domain and the terrain for the innermost domain are shown in Figure 4.

The simulations were initialized using North American Regional Reanalysis (Mesinger et al. 2006) data from the National Climate Data Center (NCDC). The fifth-order upwind-biased scheme was used in the horizontal and the

third-order upwind-biased scheme was used in the vertical within a three-stage Runge-Kutta explicit time-marching scheme. The monotonic scheme option was used for the transport of both the microphysical scalars and the TKE.

Several sensitivity runs were made for August 16, 1995. These runs were conducted to evaluate the effects of spin-up time, time step, time step for radiation calls, vertical mesh resolution, PBL scheme, and the microphysics scheme. Two different spin-up times were tested in the simulations: 1200UTC and 1800UTC on August 15, 1995. The simulations were run for 36 and 30 hours depending on initialization time for a 24hr forecast. The two different spin-up times of 6hr and 12hr were found to make little difference and therefore, a spin-up time of 6hr was used.

The time step based on the CFL criteria can be set according to:

$$\Delta t_{max} < \frac{C_{cfl}}{\sqrt{3}} \cdot \frac{\Delta x}{u_{max}} \tag{5}$$

where, C_{cfl} is the CFL criteria. If the fifth-order upwind scheme is used within a three-stage explicit Runge-Kutta time marching scheme then this constant is set to 1.42. The wind speed magnitudes in the jet stream can be substantial and therefore, u_{max} is usually set to 100m/s to insure stability. The developers of WRF also suggest using the time step according to the following relation:

$$\Delta t_{max} = c_1 \Delta x \tag{6}$$

where, $c_1 = 6s/km$ is a constant, Δx is the grid resolution in kilometers and Δt is in seconds (e.g., a Δx of 18km would suggest a $\Delta t = 108s$). In practice, however, these formulations may not work every time and the time step may need to be further reduced depending on the resolution of the vertical grid, underlying terrain, etc. In the current study it was found that the time step chosen by using both Eq. (5) and Eq. (6) was not sufficiently small enough. In some cases the simulation became unstable and stopped without giving any errors. The optimal time step required to maintain stability had to be determined by trial and error. In the simulations described in this section a time-step of 15s was used.

The Rapid Radiative Transfer Model (RRTM) longwave radiation scheme (Mlawer et al. 1997) and the Goddard shortwave scheme (Chou and Suarez 1999) were used to parameterize the effects of both longwave and shortwave radiative transfer in the atmosphere. The radiation time step was set to 4min (the suggested value for the radiation time step is 1min per 1km of grid size, e.g., it should be 10min if $\Delta x = 10km$). Different radiation time step values were tested and it was found that a higher frequency call to both longwave and shortwave radiation schemes produced a better simulation of the diurnal cycle.

The schemes tested for microphysical processes were the WRF Single-Moment 5-class scheme (details are given in the WRF User's Guide), Lin et al. (1983) scheme, and the Thompson et al. (2004) scheme. The Thompson microphysics scheme performed better compared to the Lin microphysics scheme. There were instances when the Lin microphysics scheme generated precipitation over Memphis when no precipitation was observed on ground. The use of WRF Single-Moment 5-class scheme also degraded the accuracy of the forecasts. The cumulus parameterization schemes were switched off for the simulations.

The BL and MYJ PBL schemes were tested using uniform vertical mesh resolutions of 40m, 20m, and 10m below 800m. The vertical mesh was stretched above 800m to coarser resolutions. The vertical grid levels that corresponded to these mesh resolutions were 60, 90, and 125, respectively. Increasing the vertical mesh resolution did not necessarily result in improved results. In some cases an increase in the vertical resolution degraded the quality of overall predictions.

The surface time histories of temperature and dew point temperature were noisy when the MYJ PBL scheme was used. Increasing the value of the 6th order filter coefficient suppressed the noise to a certain degree, but not completely. It should be noted that the higher-order schemes (both centered and upwind-biased) implemented in the ARW WRF model are neither TVD nor positive-definite. The transport of microphysical scalars and TKE however can be either positive-definite or monotonic.

The forecasts obtained from the sensitivity studies were compared with observations and their accuracy was quantified in terms of root mean square error, mean absolute error, and bias. The input configuration that yielded a sufficiently accurate forecast for Memphis for August 16, 1995 was used for all other days (Appendix A). Two sets of simulations were conducted (from August 15 to August 20) with all input parameters held constant except the PBL scheme. The results of these simulations are discussed in the next two sections.
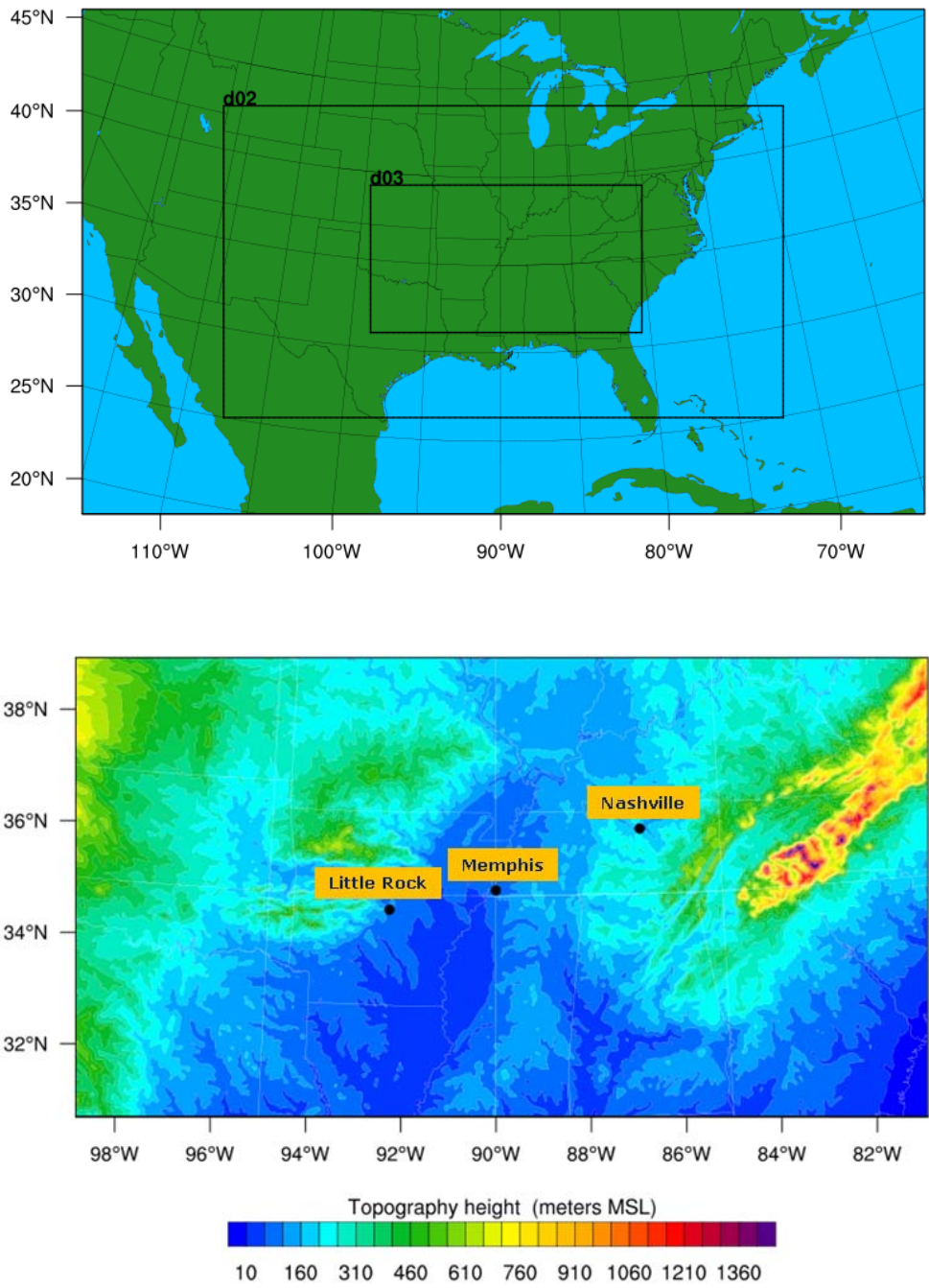
Figure 4. The top panel shows the WRF computational domain with higher resolution nests and the bottom panel shows the terrain contours for the innermost 4*km* resolution nest.

American Institute of Aeronautics and Astronautics

B. Comparison of WRF Temperature and Winds with Observations

The simulation results were compared with surface observations and upper air soundings at three locations: Memphis, Tennessee, Nashville, Tennessee and Little Rock, Arkansas. The station information is given in Table 3 and Table 4. The accuracy of simulations was quantified in terms of *root mean square error* (*Error*$_{rms}$), *mean absolute error* (*Error*$_{mae}$) and *Bias*:

$$Error_{rms} = \sqrt{\frac{1}{n}\sum_{i=1}^{n}\left(x_i^{wrf} - x_i^{obs}\right)^2} \tag{7}$$

$$Error_{mae} = \frac{1}{n}\sum_{i=1}^{n}\left|x_i^{wrf} - x_i^{obs}\right| \tag{8}$$

$$Bias = \frac{1}{n}\sum_{i=1}^{n}\left(x_i^{wrf} - x_i^{obs}\right) \tag{9}$$

The sensitivity runs were conducted for August 16, 1995, since mesoscale models are known to have difficulty in accurately simulating strongly stable nocturnal boundary layers with weak synoptic forcing (Hanna et al. 2010), as in this case.

The model preformed reasonably well and was able to simulate the main features of the diurnal cycle for August 16, 1995. The transition of the nighttime stable boundary layer to the daytime convective boundary layer was effectively simulated as well as the formation of the lower level nocturnal jet (Figure 5). With some exceptions, the surface temperature and wind predictions from the WRF model were in good agreement with observations at Memphis for the different dates.
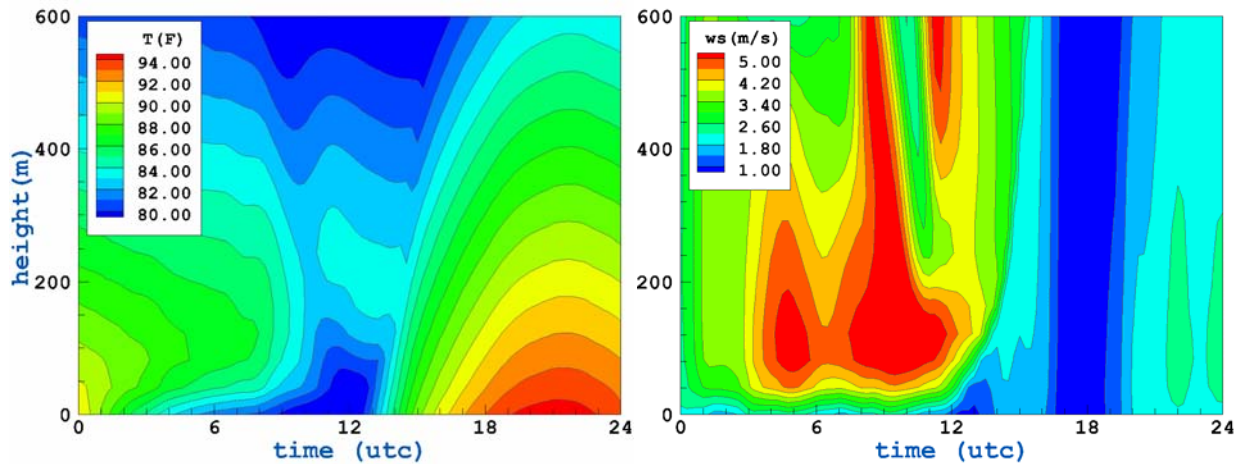

Figure 5. WRF time history at Memphis for August 16, 1995. The left panel shows the time history of temperature (°F) and the right panel shows the wind speed (m/s). MYJ PBL Scheme was used.

The WRF simulation results using the MYJ PBL scheme are compared with the surface observations from the Memphis airport and from the meteorological tower (SAVPAK) in Figures 6-7. The errors in temperature and wind velocities computed for the two sets of simulations at three different locations are tabulated in Tables 5-10. The errors at Memphis for wind velocities were fairly low, regardless of the choice for PBL schemes. The errors in temperature and dew point temperature were generally larger at Nashville and Little Rock for both PBL schemes compared to errors at Memphis. The errors in wind velocities at Nashville and Little Rock were generally low and similar to the errors at Memphis.

A closer look at the simulations suggests that the larger forecast errors present in some of the simulations (e.g., August 18) can be attributed to inadequate initialization data. These errors can be reduced by using better data assimilation and initialization techniques (e.g., observation nudging) and or a different value of spin-up time. In the case of August 18 simulation, the initialization was not improved by increasing the spin-up time to 12hr, as seen by the dashed line in Figure 6 representing 12hr spin-up time.

In some cases, the model failed to capture local subgrid scale features such as convective activity that resulted in large forecast errors. On August 17, for example, the simulated temperature and dew point temperature compared well initially with the observations, but failed to capture the sharp temperature drop at approximately 2300UTC (Figure 6). The 2m airport sensor and the 5m SAVPAK sensor show a drop of more than 10 degrees, which is not forecasted by the model.

This discrepancy between model forecast and observations was further investigated. The surface observations at Memphis recorded a thunderstorm between 2215UTC and 2323UTC with rainfall starting at 2215UTC and ending at 2310UTC. Maximum wind gusts of 9.2m/s (18kts) were recorded at the surface. The NEXRAD data over the Memphis airport at 2136UTC showed radar reflectivity (RRF) values as high as 60dBZ. Figure 8 shows the composite of lower level RRF values at different times over the Memphis airport. The echo tops were as high as 13.7km (45kft) in the vicinity of Memphis during this period. Similarly, on August 19, a thunderstorm developed between 2031UTC and 2141UTC with rainfall starting at 2107UTC and ending at 2132UTC. Maximum wind gusts of 22.1m/s (43kts) were recorded at the surface. The model was again not able to simulate this convective event. The sharp temperature drop and the increase in the observed surface winds due to the moving gust front were not captured in the model simulation (Figures 6-7). Further studies can be done to evaluate other microphysics schemes implemented in the WRF model. An increase in horizontal mesh resolution may help in resolving the small scale convective features.

Table 3: Surface Observation Stations

Location	Station ID	Latitude	Longitude	Elevation
Memphis, TN	MEM	35.042°N	89.976°W	103.9m
Nashville, TN	BNA	36.124°N	86.678°W	182.6m
Little Rock, AR	LIT	34.729°N	92.224°W	79.9m

Table 4: Upper Air Soundings

Location	Station ID	Latitude	Longitude	Elevation
Memphis, TN	MEM	35.029°N	89.981°W	97.37m
Nashville, TN	BNA	36.25°N	86.55°W	210m
Little Rock, AR	LZK	34.72°N	92.23°W	78m

The comparisons of upper air soundings from WRF and Memphis on August 16, 1995 are shown in Figures 9-12. Also shown are the comparison of the predicted WRF wind speed and direction with the profile generated by Lincoln Labs. The Lincoln Labs profile, in which data measured from several different types of instruments was fused together to generate a single profile, agrees well with the model simulations (Figures 9-10). The low-ascent field experiment sounding data which was at a much higher resolution is plotted for Memphis in Figure 11.
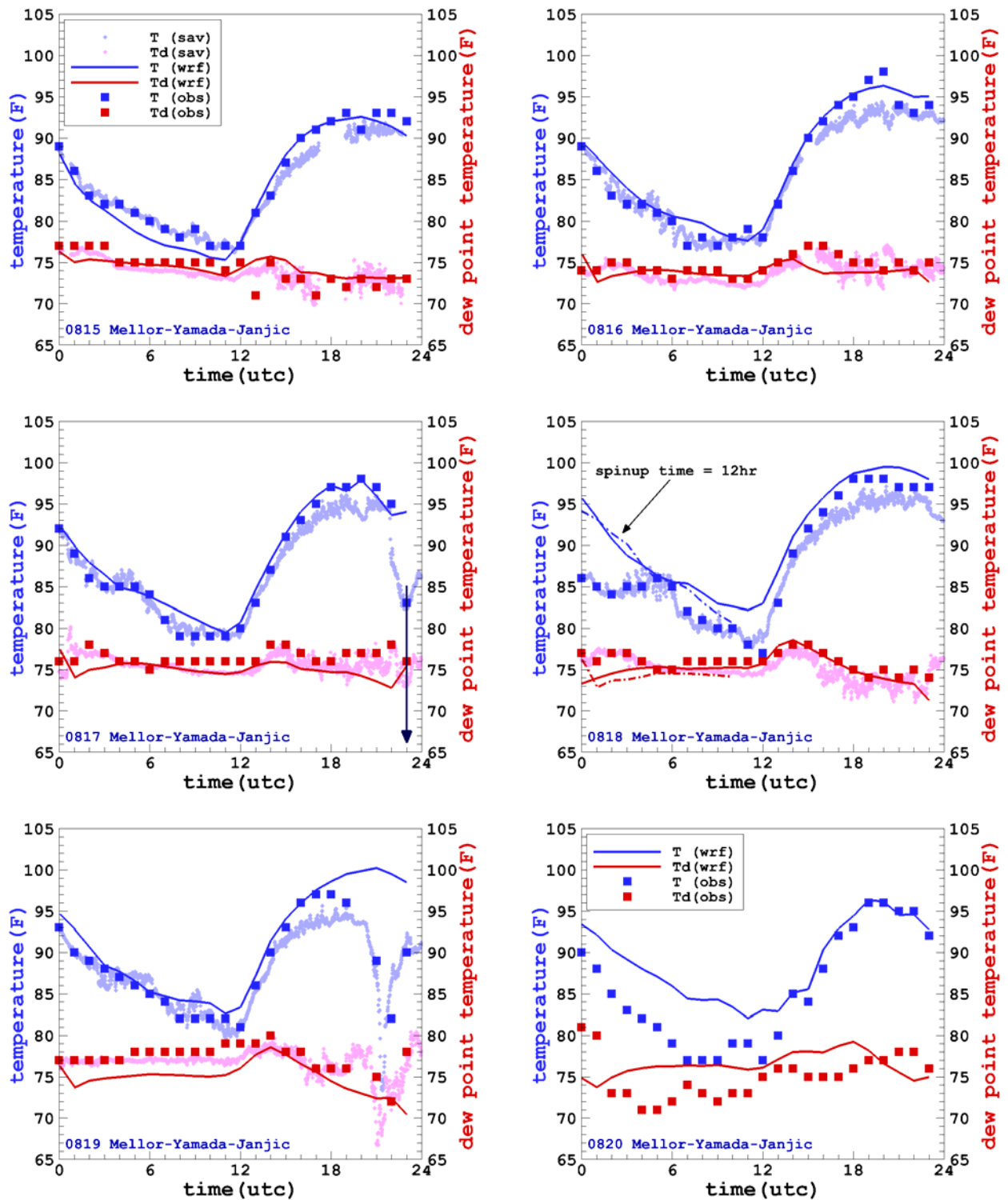
Figure 6. Comparison of WRF simulations with observations. Observed temperatures at 2*m* for Memphis are shown as squares and the SAVPAK 5*m* data is given by small diamonds in the figure. The SAVPAK data frequency is every one minute. WRF simulation results are denoted by solid lines. The SAVPAK data was not available for August 20, 1995.

Figure 7. Comparison of WRF simulations with observations. Observed winds at 10*m* **for Memphis are depicted by squares and the 5***m* **SAVPAK data is given by small diamonds in the figure. The SAVPAK data frequency is every one minute. WRF simulation results are denoted by solid lines. The SAVPAK data was not available for August 20, 1995.**
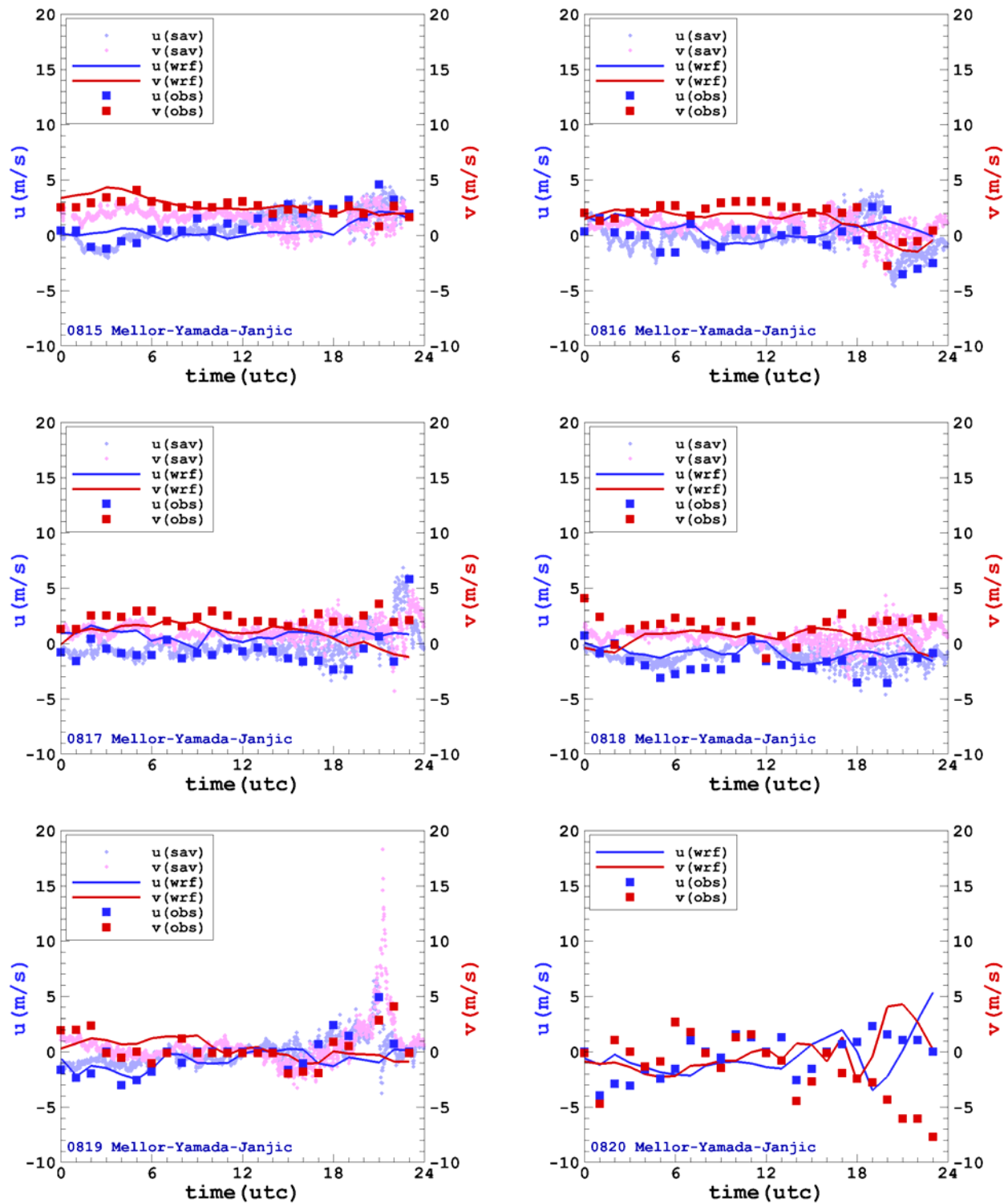
Table 5: Memphis, Tennessee (Bougeault-Lacarreré Scheme)

date	T(°F)			T_d(°F)			u(m/s)			v(m/s)		
	rmse	mae	bias	rmse	mae	bias	rmse	mae	bias	rmse	mae	bias
950815	1.17	0.96	-0.27	2.08	1.69	0.77	1.25	1.04	-0.72	0.54	0.45	-0.20
950816	**1.53**	**1.25**	**0.96**	**1.28**	**0.99**	**-0.58**	**1.52**	**1.19**	**0.52**	**0.92**	**0.71**	**-0.31**
950817	3.05	1.74	1.62	1.60	1.25	-0.99	2.03	1.70	1.22	1.64	1.31	-1.26
950818	3.80	3.07	3.07	1.15	0.96	-0.14	1.36	1.12	1.07	1.61	1.24	-1.00
950819	4.03	2.19	2.17	2.20	1.87	-1.14	1.60	1.21	-0.47	1.65	1.31	0.07
950820	4.76	4.38	3.54	3.06	2.71	1.69	1.97	1.63	-0.04	2.78	2.35	0.55

August 16, 1995 (950816) was used for the different sensitivity runs.

Table 6: Nashville, Tennessee (Bougeault-Lacarreré Scheme)

date	T(°F)			T_d(°F)			u(m/s)			v(m/s)		
	rmse	mae	bias	rmse	mae	bias	rmse	mae	bias	rmse	mae	bias
950815	2.52	2.24	1.86	2.86	2.53	-2.31	1.75	1.56	1.11	2.05	1.81	0.63
950816	2.43	1.96	1.88	2.28	1.82	1.35	2.03	1.58	-0.31	1.86	1.55	0.57
950817	1.84	1.55	1.49	1.07	0.83	0.59	1.94	1.51	-0.80	1.41	1.15	0.79
950818	5.95	3.58	3.26	2.49	2.22	2.17	2.05	1.65	-1.42	2.52	1.66	0.30
950819	6.34	5.80	4.59	3.68	3.29	3.29	2.34	1.90	-1.65	2.30	1.95	-0.37
950820	2.81	2.47	2.47	4.84	4.12	3.39	2.59	1.87	-0.79	2.55	2.06	0.05

Table 7: Little Rock, Arkansas (Bougeault-Lacarreré Scheme)

date	T(°F)			T_d(°F)			u(m/s)			v(m/s)		
	rmse	mae	bias	rmse	mae	bias	rmse	mae	bias	rmse	mae	bias
950815	2.39	2.07	-0.85	4.10	3.08	2.36	1.90	1.61	-0.62	0.79	0.60	-0.01
950816	2.03	1.61	-0.91	2.76	2.44	0.73	2.04	1.82	0.54	1.29	1.05	-0.08
950817	2.89	2.25	-1.43	3.62	2.78	1.48	2.75	2.31	2.03	2.11	1.81	-0.03
950818	2.57	1.61	-1.35	1.92	1.69	-0.68	2.84	2.70	2.11	1.97	1.57	-0.49
950819	4.50	3.10	-3.07	2.52	1.84	0.56	3.11	2.60	1.33	2.07	1.69	-0.06
950820	3.81	3.38	2.14	4.27	3.90	3.83	1.44	1.21	0.11	2.29	1.72	0.91

American Institute of Aeronautics and Astronautics

Table 8: Memphis, Tennessee (Mellor-Yamada-Janjić Scheme)

date	T(°F)			T_d(°F)			u(m/s)			v(m/s)		
	rmse	mae	bias	rmse	mae	bias	rmse	mae	bias	rmse	mae	bias
950815	1.43	1.23	-0.76	1.42	1.02	0.11	1.41	1.21	-0.76	0.58	0.48	0.21
950816	1.40	1.15	0.81	1.37	1.02	-0.66	1.68	1.32	0.74	0.88	0.74	-0.43
950817	2.56	1.43	1.11	1.98	1.63	-1.46	2.15	1.84	1.43	1.68	1.36	-1.33
950818	3.87	3.07	3.07	1.38	1.04	-0.84	1.25	0.98	0.86	1.78	1.40	-1.12
950819	4.92	2.80	2.79	2.76	2.34	-2.30	1.73	1.12	-0.48	1.60	1.21	-0.04
950820	4.39	3.53	3.46	3.43	3.05	1.41	2.48	2.03	-0.16	4.26	3.09	1.43

August 16, 1995 (950816) was used for the different sensitivity runs.

Table 9: Nashville, Tennessee (Mellor-Yamada-Janjić Scheme)

date	T(°F)			T_d(°F)			u(m/s)			v(m/s)		
	rmse	mae	bias	rmse	mae	bias	rmse	mae	bias	rmse	mae	bias
950815	2.24	1.94	1.58	3.24	2.87	-2.85	1.82	1.66	1.43	2.01	1.75	0.63
950816	2.22	1.83	1.55	2.26	1.91	0.59	1.95	1.44	0.01	2.17	1.83	1.16
950817	1.89	1.60	1.54	0.84	0.69	-0.28	1.88	1.47	-0.91	1.65	1.35	0.79
950818	5.78	3.43	3.08	1.50	1.29	0.93	2.03	1.64	-1.38	2.61	1.90	0.21
950819	6.85	6.31	3.22	3.45	3.25	3.25	3.48	2.47	-2.34	2.42	2.20	-0.38
950820	3.13	2.64	2.02	5.42	4.57	4.32	2.25	1.78	-0.98	2.05	1.73	0.04

Table 10: Little Rock, Arkansas (Mellor-Yamada-Janjić Scheme)

date	T(°F)			T_d(°F)			u(m/s)			v(m/s)		
	rmse	mae	bias	rmse	mae	bias	rmse	mae	bias	rmse	mae	bias
950815	2.43	2.00	-1.04	3.70	2.92	2.04	1.70	1.42	-0.36	0.92	0.70	0.002
950816	2.25	1.75	-1.13	2.21	1.93	0.55	2.10	1.78	0.84	1.23	0.99	-0.04
950817	3.04	2.35	-1.93	3.24	2.42	1.21	2.91	2.49	1.94	2.18	1.84	-0.01
950818	2.61	1.96	-0.80	1.47	1.29	-0.05	2.90	2.63	2.37	2.03	1.65	-0.69
950819	5.18	3.60	-3.46	1.91	1.42	1.27	2.98	2.45	2.01	1.88	1.38	0.007
950820	3.17	2.73	0.63	4.03	3.66	3.54	1.86	1.51	-0.09	3.00	2.35	1.05

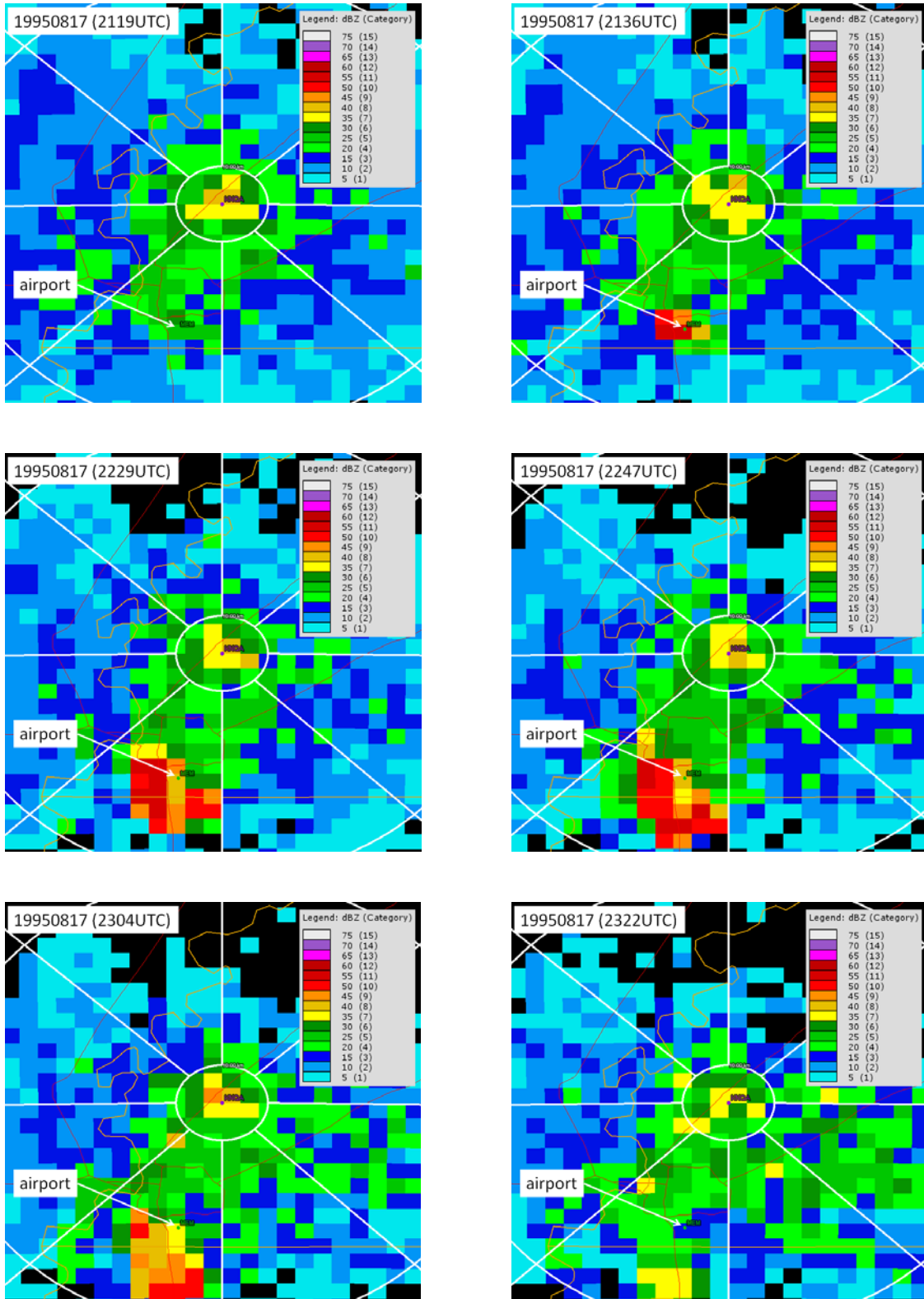American Institute of Aeronautics and Astronautics

Figure 8. Memphis NEXRAD data for August 17, 1995. NEXRAD Site ID: KNQA. The composite of lower level radar reflectivity at different times is shown in the figure. The start of convective activity over the Memphis International Airport is after 2119UTC. Areas of high radar reflectivity (> 60*dBZ*) can be seen in the vicinity of the airport.
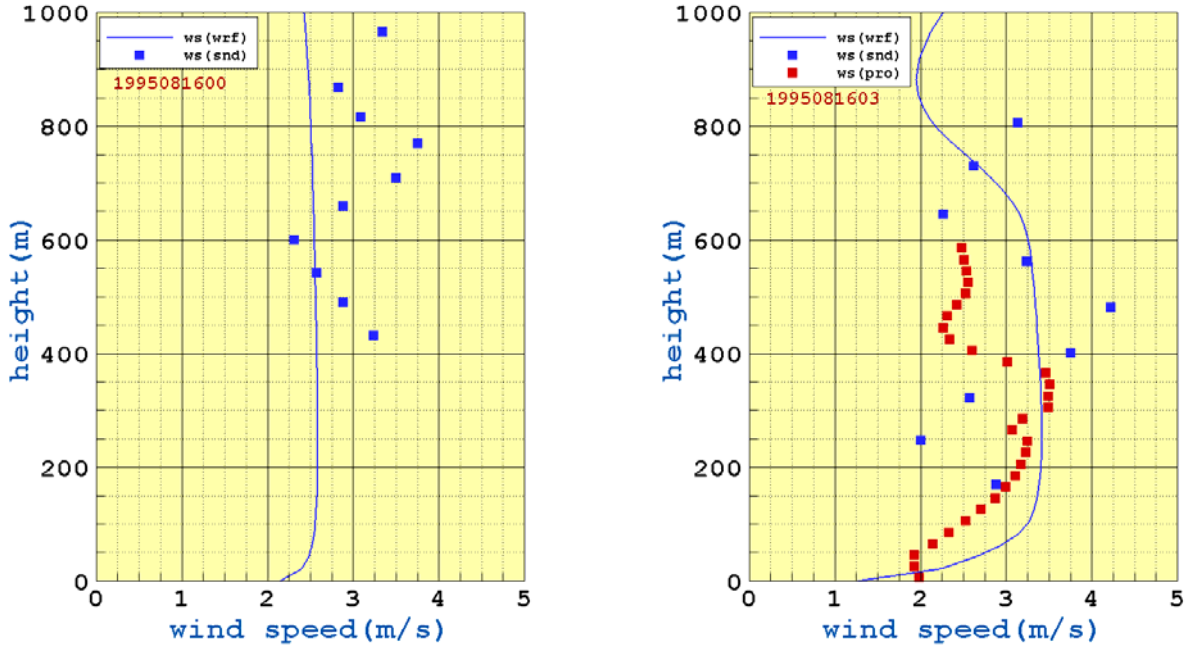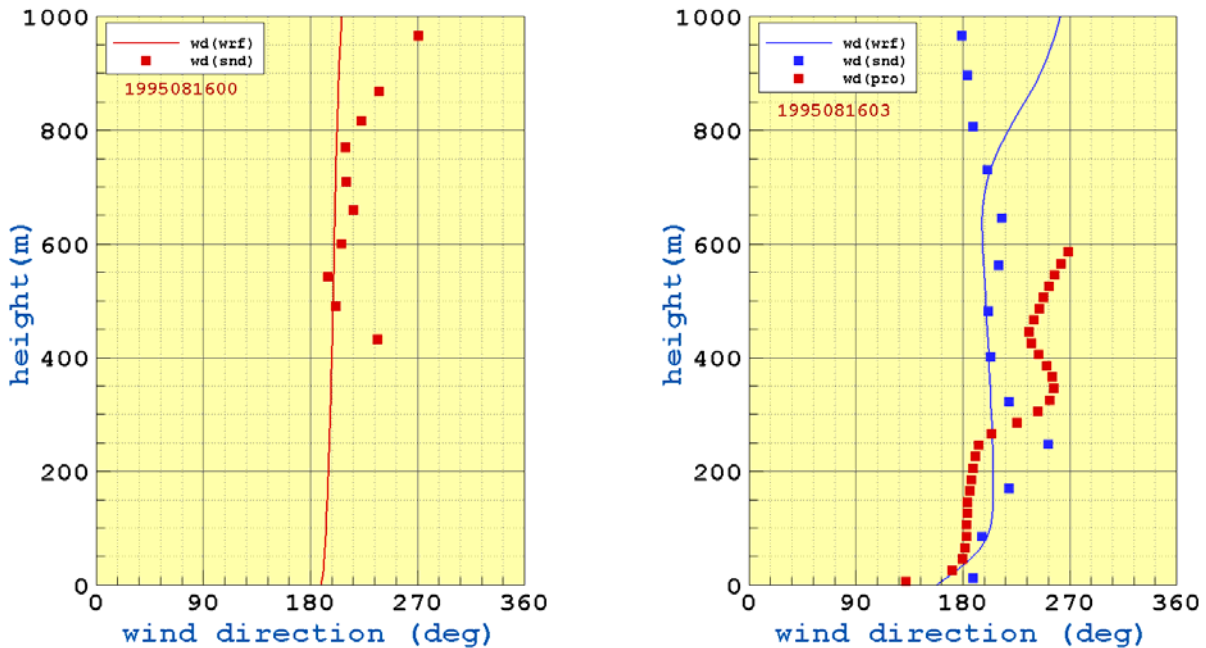
Figure 9. Comparison of WRF simulation data with observations (August 16, 1995). Wind speed profile for Memphis at time = 6hr into the simulation is shown in the left panel and at time = 9hr into the simulation is shown in the right panel. Points are observations and solid lines are WRF computations. Red points in the right panel correspond to the profile generated by Lincoln Labs which fused the data measured from several different types of instruments.
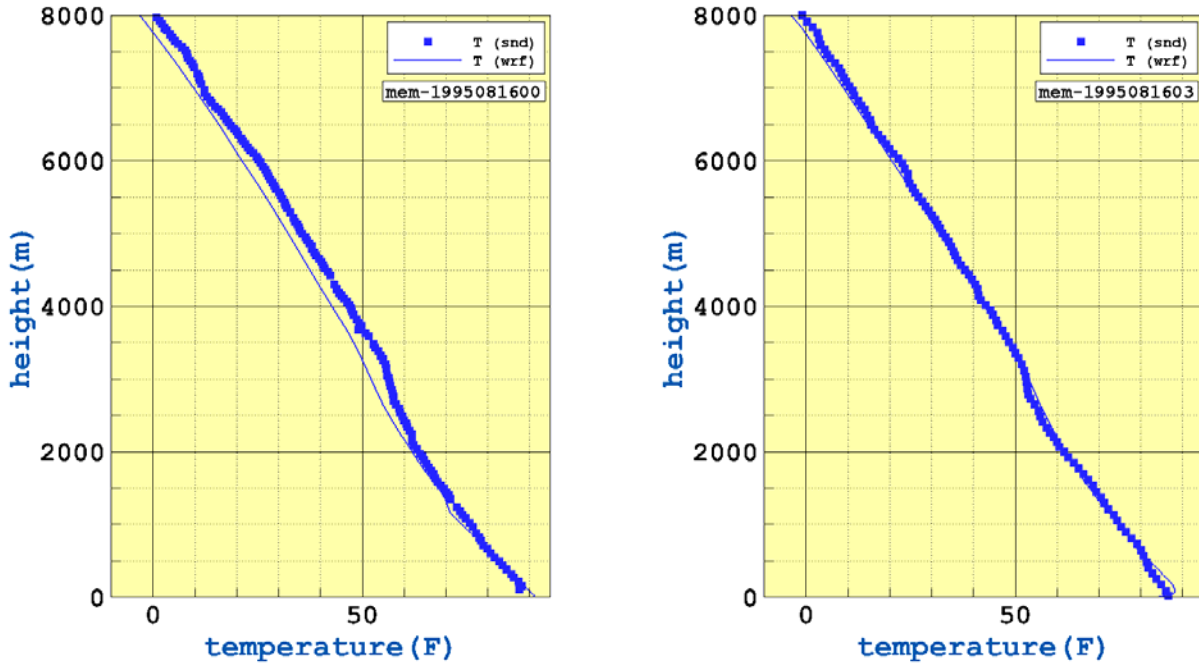

Figure 10.   Comparison of WRF simulation data with observations (August 16, 1995). Wind direction profile for Memphis at time = 6hr into the simulation is shown in the left panel and at time = 9hr into the simulation is shown in the right panel. Points are observations and solid lines are WRF computations. Red points in the right panel correspond to the profile generated by Lincoln Labs which fused the data measured from several different types of instruments.

Figure 11. Comparison of WRF simulation data with observations (August 16, 1995). Vertical temperature profile for Memphis at time = *6hr* into the simulation is shown in the left panel and at time = *9hr* into the simulation is shown in the right panel. Points are observations and solid lines are WRF computations.
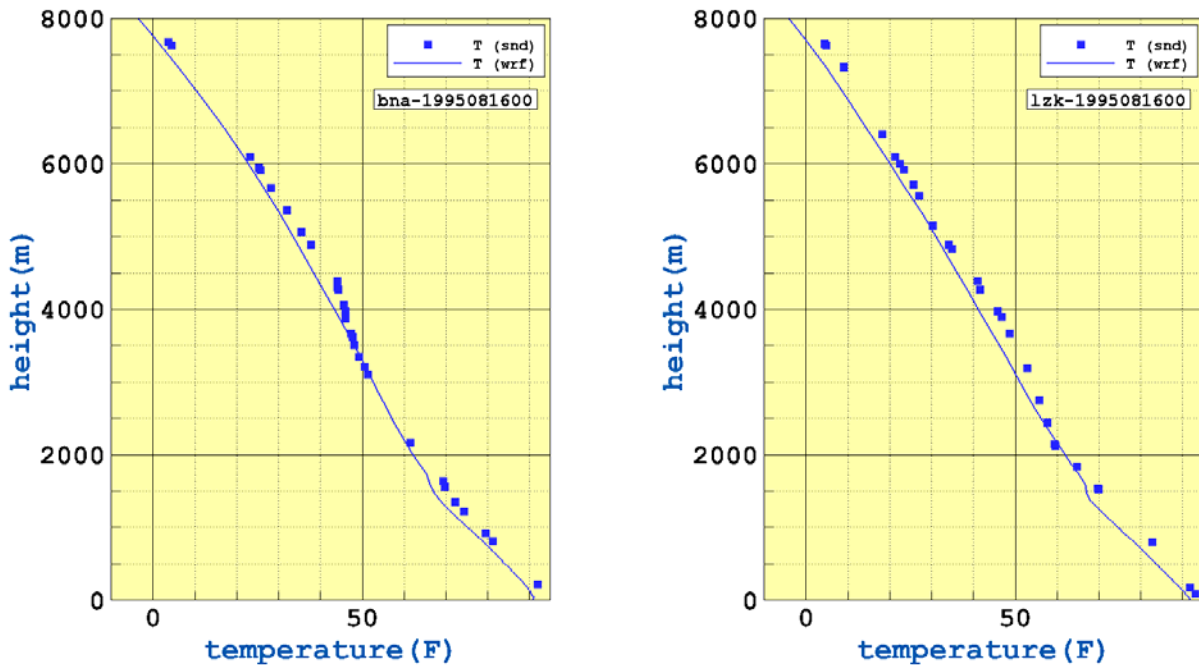
Figure 12. Comparison of WRF simulation data with observations (August 16, 1995). Vertical temperature profile for Nashville at time = *6hr* into the simulation is shown in the left panel and for Little Rock at time = *6hr* into the simulation is shown in the right panel. Points are observations and solid lines are WRF computations.

C. Comparison of Model derived EDR with measured EDR

The EDR is diagnosed from WRF model output of TKE and the master length scale. Previous studies have shown that the use of model predicted master length scale in EDR calculation results in large errors. Some researchers have suggested using a constant value of length scale for EDR calculation, therefore, in addition to the EDR calculated using the model output of the master length scale, three different values of a constant length scale were also tested. The constant values used were $336m$ as suggested by Ringley et al. (2007); $311m$ suggested by Frech et al. (2007) and $300m$. The use of different values of a constant length scale did not change the EDR values significantly. The errors in the TKE and EDR computed for the two sets of WRF simulations (using the BL and the MYJ PBL schemes) are given in Tables 11-12. The EDR in the tables was calculated using both the constant length scale ($300m$) as well as the model output of length scale. In general the errors were smaller when the MYJ PBL scheme was used and errors were smaller when a constant value of the length scale was used instead of the model output of the length scale. The errors listed in Tables 11-12 were computed using only the data points between 1200UTC and 2400UTC which roughly corresponds to the daytime well-mixed convective boundary layer. The FLUXPAK data was not available for the daytime hours of August 15, 1995. On August 17 and August 19, 1995, the spike in both TKE and the EDR occurs around the time of convective activity which was not captured by the model. This resulted in large errors in TKE and EDR predictions on these two dates for both PBL schemes.

Compared to the RMS errors in EDR predictions reported by Frech et al. (2007) which were on the order of $0.004m^2/s^3$, the RMS errors in EDR using MYJ scheme for the current study are an order of magnitude lower when using a constant length scale. Ringley at al. (2007) also conducted an extensive evaluation of the MASS model predictions of TKE and EDR against the 1997 AVOSS data collected at the Dallas-Fort Worth Airport. They did not report quantitative measures such as RMSE but instead provided plots of model predicted TKE and EDR compared with measurements. The plots given in Ringley et al. (2007) indicate a model underestimation of TKE by as much as 75% in the nighttime boundary layer. There are also large errors in EDR predictions during both the daytime and the nighttime boundary layer. In their evaluation of mesoscale models for dispersion applications, Hanna et al. (2010) noted that the TKE and other boundary layer parameters were "least well simulated on very stable nights" when the models default to the threshold values of TKE. The Nonhydrostatic Mesoscale Model (WRF-NMM) and the MM5 model were used in their study. For the daytime boundary layer, the TKE predictions were usually within a factor of two of the observations with degradation in nighttime predictions. On average they found that the WRF-NMM and MM5 predictions underestimated the TKE by 20-50%.

The WRF simulation results of TKE and EDR using the MYJ PBL scheme are compared with the met tower observations (FLUXPAK) in Figures 13-14. The WRF prediction for the daytime convective boundary layer matches the observed data fairly well. However, the results for the nighttime stable boundary layer were overestimated (solid black lines in Figures 13-14). An increase in the vertical mesh resolution resulted in an improvement for the nighttime prediction of EDR by the BL PBL scheme. In the case of MYJ PBL scheme, however, an increase in the vertical mesh resolution slightly improved the results for the nighttime predictions but degraded the quality of the overall forecast. In general, grid convergence could not be achieved for either scheme.

The simulation results showed that during the nighttime stable boundary layer the model often defaulted to a threshold value for the TKE which was too large. The threshold values are typically used in the absence of sufficient instability and wind shear to ensure non-zero TKE. This resulted in large values of EDR during the nighttime stable boundary layer (solid black lines in Figure 14). For wake applications this would imply a prediction of rapid vortex decay. Janjić (personal communications) suggested using a lower value for the TKE threshold. The floor value of TKE was decreased in the WRF code from $10^{-1}m^2/s^2$ to $10^{-2}m^2/s^2$ and the simulations were performed again. The results for the modified code are depicted by the dashed orange lines in Figures 13-14. The results for August 16, 1995 showed substantial improvement in both the TKE and EDR predictions and for other days gave a conservative prediction for EDR. In general, the decrease in the TKE threshold resulted in either an approximately average value or an underestimation of EDR for the nighttime stable boundary layer. The conservative prediction of EDR in this case was based on a realistic TKE threshold value and is also desirable for operational safety concerns. A lower value of EDR implies larger wake decay times and adds toward the factor of safety in the fast-time wake model predictions.

Finally it should be noted that although this study was conducted to evaluate the two PBL schemes in the WRF model, the strong coupling of various physics and dynamics modules with each other makes it difficult to isolate the performance of one specific module or scheme. The current study reflects the performance of the two PBL schemes as implemented in the ARW version of the WRF model. Further studies can be conducted to evaluate other mesoscale models such as the WRF-NMM from NCEP and the Operational Multiscale Environment model with Grid Adaptivity (OMEGA).

Table 11: Memphis, Tennessee (Bougeault-Lacarreré Scheme)

date	TKE(m^2/s^2)			EDR_{Lw}(m^2/s^3)			EDR_{Lc}(m^2/s^3)		
	rmse	mae	bias	rmse	mae	bias	rmse	mae	bias
950816	0.69	0.56	0.51	0.005	0.004	0.004	0.004	0.003	0.003
950817	1.16	0.74	0.22	0.006	0.004	0.003	0.005	0.003	0.002
950818	0.53	0.40	0.29	0.005	0.003	0.003	0.004	0.003	0.002
950819	1.71	0.88	-0.02	0.02	0.007	-0.0005	0.02	0.006	-0.001
950820	0.72	0.56	0.25	0.007	0.005	0.005	0.005	0.004	0.004

EDR_{Lw} = EDR calculated using the length scale from model output
EDR_{Lc} = EDR calculated using a constant length scale of 300*m*

Table 12: Memphis, Tennessee (Mellor-Yamada-Janjić Scheme)

date	TKE(m^2/s^2)			EDR_{Lw}(m^2/s^3)			EDR_{Lc}(m^2/s^3)		
	rmse	mae	bias	rmse	mae	bias	rmse	mae	bias
950816	0.35	0.19	-0.07	0.0009	0.0007	-0.0007	0.0006	0.0004	0.0003
950817	1.18	0.52	-0.50	0.002	0.001	-0.001	0.002	0.001	-0.0006
950818	0.36	0.27	-0.25	0.001	0.001	0.0007	0.0005	0.0003	-0.00003
950819	1.58	0.54	-0.42	0.02	0.005	-0.002	0.02	0.004	-0.003
950820	0.58	0.40	-0.32	0.001	0.001	0.001	0.001	0.0008	0.0006

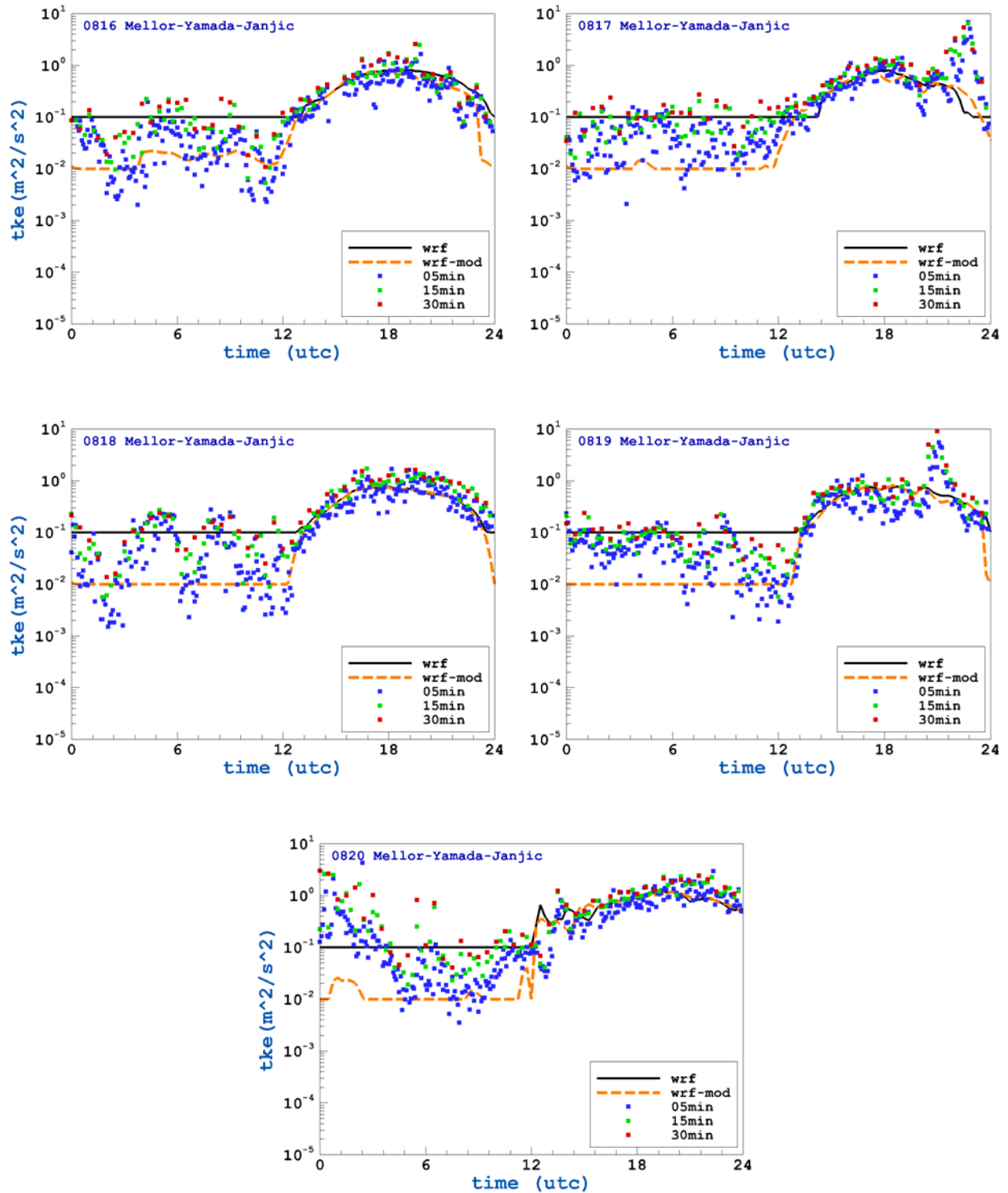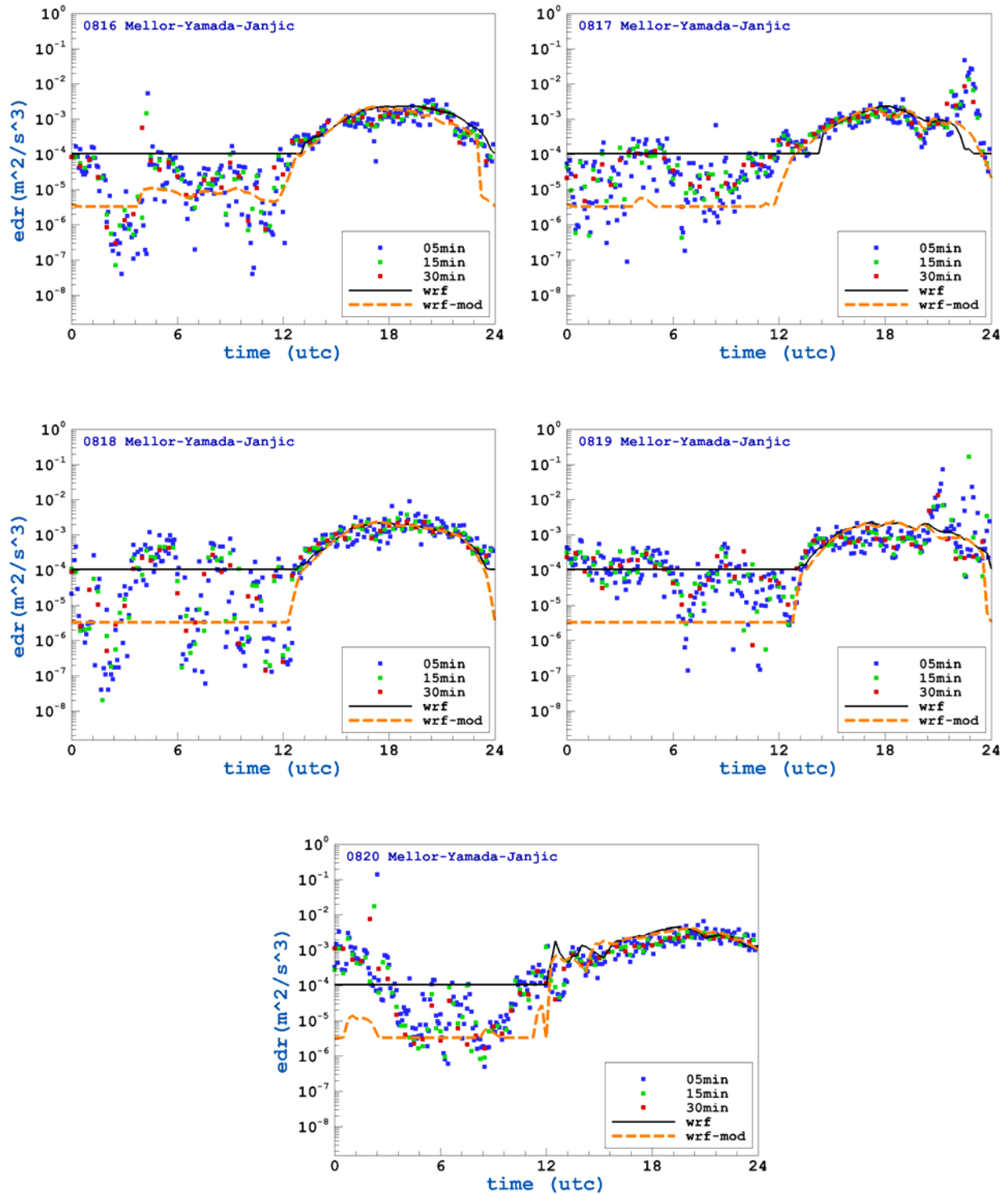American Institute of Aeronautics and Astronautics

Figure 13. Comparison of simulated TKE values with observed data. Simulation results using the Mellor-Yamada-Janjić (MYJ) PBL scheme are shown for different dates. Points represent observations taken within three different time windows (5*min*, 15*min* and 30*min*). WRF computations are given by lines. Δz=40*m*.

Figure 14. Comparison of simulated EDR values with observed data. Simulation results using the Mellor-Yamada-Janjić (MYJ) PBL scheme are shown for different dates. Points represent observations taken within three different time windows (5*min*, 15*min* and 30*min*). WRF computations are given by lines. Δ*z*=40*m*.

American Institute of Aeronautics and Astronautics

VI. Summary

Several simulations were conducted using different physics options and model run configurations. The WRF model was able to capture the main features of the complete diurnal cycle such as the development of a low level jet during the nighttime stable boundary layer and the transition of the nighttime stable boundary layer into the daytime convective boundary layer. The forecasts of surface temperature and winds compared favorably both qualitatively and quantitatively with observations. The cases with large errors in the model forecasts were either due to poor initialization or due to model's inability to capture local subgrid-scale convective activity.

The TKE and the EDR predictions compared well with observations for the daytime convective boundary layer, but large errors were observed for the nighttime stable boundary layer. The BL PBL scheme underestimated the EDR during the nighttime and the MYJ PBL scheme overestimated EDR during the nighttime. An increase in the vertical mesh resolution did not give consistent improvement in predictions and in some cases degraded the accuracy of the overall forecast. In general, grid convergence could not be achieved for either scheme. Decreasing the value of TKE threshold for the MYJ PBL scheme resulted in more realistic EDR predictions for the nighttime boundary layer. Overall, the errors were smaller when the MYJ PBL scheme was used compared to the BL PBL scheme and errors were smaller when a constant value of the length scale was used instead of the model predicted length scale.

The mesoscale models have proved invaluable for meteorological forecast and analysis and for detailed forensic reconstruction of events of interest. The errors in temperature and wind forecasts have been reduced significantly over the years but in their current state they are not recommended for real-time predictions of turbulence parameters such as EDR to support terminal area operations. Further research leading to improvements in PBL closure schemes is needed, especially for accurate simulations of the nighttime stable boundary layer with weak synoptic forcing.

Appendix A

The main input parameters used in the simulations are listed in this appendix. These parameters were held constant for the two sets of simulations using the Mellor-Yamada-Janjić (MYJ) and the Bougeault and Lacarreré (BL) schemes. The values used in some of the sensitivity studies for August 16, 1995 are shown in bold font.

- Time-marching: 3rd order Runge-Kutta
- Time step: 15s
    - **20s, 30s, 60s**
- Momentum advection: 5th order upwind in the horizontal and 3rd order upwind in the vertical
- $\Delta x = \Delta y = 4km$
- Number of vertical levels: 60
    - **90, 125**
- Vertical mesh resolution (Δz) near surface: 40m
    - **20m, 10m**
- Longwave Radiation Scheme: RRTM
- Shortwave Radiation Scheme: Goddard
- Radiation call: 4min
    - **2min, 10min**
- Microphysics Scheme: Thompson
    - **Lin, WRF Single-Moment 5-class**
- Advection of TKE and microphysical scalars: Monotonic
    - **Positive-definite**
- Model initialization using the NARR data from NCDC
- Spin-up Time: 6hr
    - **12hr**

Acknowledgments

References

Arakawa, A., V. R. Lamb, "Computational design of the basic dynamical process of the UCLA general circulation model", *Methods in Computational Physics*, Vol. 17, 1977, pp. 173-265.

Bacon, D. P., N. N. Ahmad, Z. Boybeyi, T. J. Dunn, M. S. Hall, P. C. S. Lee, R. A. Sarma, M. D. Turner, K. Waight, S. Young, and J. Zack, "A Dynamically Adapting Weather and Dispersion Model: The Operational Multiscale Environment Model with Grid Adaptivity (OMEGA)", *Monthly Weather Review*, Vol. 128, 2000, pp. 2044-2076.

Benjamin, S. G., G. G. Grell, J. M. Brown, T. G. Smirnova, R. Bleck, "Mesoscale Weather Prediction with the RUC Hybrid Isentropic-Terrain-Following Coordinate Model", *Monthly Weather Review*, Vol. 132, 2004, pp. 473-494.

Blackadar, A. K., "High resolution models of the planetary boundary layer", *Advances in Environmental Science and Engineering*, Vol. 1, 1979, pp. 50-85.

Bougeault, G., and P. Lacarrère, "Parameterization of Orography-Induced Turbulence in a Mesobeta-Scale Model", *Monthly Weather Review*, Vol. 117, 1989, pp. 1872-1890.

Burk, S. D., and W. T. Thompson, "A vertically nested regional numerical prediction model with second-order closure physics", *Monthly Weather Review*, Vol. 117, 1989, pp. 2305-2324.

Campbell, S.D., et al., "Wake Vortex Field Measurement Program at Memphis, TN Data Guide", Lincoln Laboratory, Massachusetts Institute of Technology. Project Report NASA/L-2. 1997.

Charney, J. J., M. L. Kaplan, Y. Lin, K. D. Pfeiffer, "A New Eddy Dissipation Rate Formulation for the Terminal Area PBL Prediction System (TAPPS)", AIAA-2000-0624.

Chou, M. D., and M. J. Suarez, "A solar radiation parameterization for atmospheric studies", NASA Technical Report NASA/TM-1999-10460. 1999.

Dudhia, J., "A nonhydrostatic version of the Penn State/NCAR mesoscale model: Validation tests and simulation of an Atlantic cyclone and cold front", *Monthly Weather Review*, Vol. 121, 1993, pp. 1493-1513.

Frech, M., F. Holzäpfel, A. Tafferner, T. Gerz, "High-Resolution Weather Database for the Terminal Area of Frankfurt Airport", *Comptes Rendus Physique*, Vol. 6, 2005, pp. 501-523.

Gerz, T., F. Holzäpfel, W. Bryant, F. Köpp, M. Frech, A. Tafferner, G. Winckelmans, "Research towards a wake vortex advisory for optimal aircraft spacing", *Journal of Applied Meteorology and Climatology*, Vol. 46, 2007, pp. 1913-1932.

Han, J., S. P. Arya, S. Shen, Y. Lin, "An Estimation of Turbulent Kinetic Energy and Energy Dissipation Rate Based on Atmospheric Boundary Layer Similarity Theory", NASA Contractor Report NASA-CR-2000-210298. 2000.

Hanna, S., B. Reen, E. Hendrick, L. Santos, D. Stauffer, A. Deng, J. McQueen, M. Tsidulko, Z. Janjić, D. Jović, R. I. Sykes, "Comparison of Observed, MM5 and WRF-NMM Model-Simulated, and HPAC-Assumed Boundary-Layer Meteorological Variables for 3 Days During the IHOP Field Experiment", *Boundary Layer Meteorology*, Vol. 134, 2010, pp. 285-306.

Hinton, D. A., "Aircraft Vortex Spacing System (AVOSS) Conceptual Design", NASA Technical Memorandum NASA-TM-110184, 1995.

Holzäpfel, F. and R.E. Robins, "Probabilistic Two-Phase Aircraft Wake-Vortex Model: Application and Assessment," *Journal of Aircraft*, Vol. 41, 2004, pp. 1117-1126.

Holzäpfel, F., "Minutes of the WakeNet3-Europe Workshop on Short-Term Weather Forecasting for Probabilistic Wake-Vortex Prediction", Institut für Physik der Atmosphäre, Duetsches Zentrum für Luft- und Raumfahrt. April 2010.

Hodur, R.M., "The Naval Research Laboratory's Coupled Ocean/Atmosphere Mesoscale Prediction System (COAMPS)", *Monthly Weather Review*, Vol. 125, 1997, pp. 1414-1430.

Janjić, Z., "The Step-Mountain Eta Coordinate Model: Further Developments of the Convection, Viscous Sublayer, and Turbulence Closure Schemes", *Monthly Weather Review*, Vol. 122, 1994, pp. 927-945.

Janjić, Z., "Nonsingular implementation of the Mellor-Yamada Level 2.5 scheme in the NCEP Meso model", NCEP Office Note No. 437. pp. 61.

Kaplan, M. L., Y. Lin, C. J. Ringley, Z. G. Brown, M. T. Kiefer, P. S. Suffern, A. M. Hoggarth, "Wake Vortex Environment Simulations from a Terminal Area PBL Prediction System (TAPPS)", AIAA-2006-1074.

Kaplan, M. L., R. P. Weglarz, Y. Lin, D. B. Ensley, J. K. Kehoe, D. Decroix, "A Terminal Area PBL Prediction System for DFW", AIAA-1999-0983.

Klemp, J. B., W. C. Skamarock, and J. Dudhia, "Conservative Split-Explicit Time Integration Methods for the Compressible Nonhydrostatic Equations," *Monthly Weather Review*, Vol. 135, August 2007, pp. 2897-2913.

Lin, Y-L., Farley, R. D., and Orville, H. D., "Bulk parameterization of the snow field in a cloud model", *Journal of Climate and Applied Meteorology,* Vol. 22, 1983, pp. 1065-1092.

Mellor, G. L., and T. Yamada, "Development of a turbulence closure model for geophysical fluid problems", *Reviews of Geophysics and Space Physics*, Vol. 20, 1982, pp. 851-875.

Mesinger, F., G. DiMego, E. Kalnay, K. Mitchell, P. C. Shafran, W. Ebisuzaki, D. Jović, J. Woollen, E. Rogers, E. H. Berbery, M. B. Ek, Y. Fan, R. Grumbine, W. Higgins, H. Li, Y. Lin, G. Manikin, D. Parrish, W. Shi,"North American Regional Reanalysis", *Bulletin of the American Meteorological Society*, Vol. 87, 2006, pp. 343-360.

MESO Inc., "MASS Reference Manual Version 5.10", 1995. 129 pp. Available from MESO Inc., 185 Jordan Road, Troy, New York 12180.

Mesoscale and Microscale Meteorology Division, "Weather Research & Forecasting ARW Version 3 Modeling System User's Guide", 2010, 352 pp. National Center for Atmospheric Research.

Mlawer, E. J., S. J. Taubman, P. D. Brown, M. J. Iacono, and S. A. Clough, "Radiative transfer for inhomogeneous atmosphere: RRTM, a validated correlated-k model for the longwave", *Journal of Geophysical Research*, Vol. 102, 1997, pp. 663-682.

Nakanishi, M., and H. Niino, "An Improved Mellor-Yamada Level-3 Model with Condensation Physics: Its Design and Verification", *Boundary Layer Meteorology*, Vol. 112, 2004, pp. 1-31.

Perry, R. B., D.A. Hinton, and R.A. Stuever, "NASA Wake Vortex Research for Aircraft Spacing," AIAA-1997-0057.

Proctor, F.H., D. W. Hamilton, G. F. Switzer, "TASS Driven Algorithms for Wake Prediction", AIAA-2006-1073.

Proctor, F.H., "Evaluation of Fast-Time Wake Vortex Prediction Models", AIAA-2009-0344.

Ringley, C. J., Y. Lin, Z. G. Brown, M. L. Kaplan, "The Development of a Boundary Layer Turbulence Database for Wake Vortex Applications", AIAA-2007-287.

Sarpkaya, T., R.E. Robins, and D.P. Delisi, "Wake-Vortex Eddy-Dissipation Model Predictions Compared with Observations," *Journal of Aircraft*, Vol. 38, 2001, pp. 687- 692.

Therry, G., and P. Lacarrère, "Improving the Eddy Kinetic Energy Model for Planetary Boundary Layer Description", *Boundary Layer Meteorology*, Vol. 25, 1983, pp. 63-88.

Thompson, G., R. M. Rasmussen, K. Manning, "Explicit Forecasts of Winter Precipitation using an Improved Bulk Microphysics Scheme. Part1: Description and Sensitivity Analysis", *Monthly Weather Review*, Vol. 132, 2004, pp. 519-542.

Troen, I., and L. Mahrt, "Simple model of the atmospheric boundary layer; sensitivity to surface evaporation", *Boundary Layer Meteorology*, Vol. 37, 1986, pp. 129-148.

Yamada, T., and G. Mellor, "A Simulation of the Wangara Atmospheric Boundary Layer Data", *Journal of Atmospheric Sciences*, Vol. 32, 1975, pp. 2309-2329.

Zak, J. A., "Cases of Interesting Meteorological Conditions during Wake Vortex Measurements at Memphis, Tennessee during August 1995", Vigyan Interim Report for NASA Contract NAS1-19341. 1996.